Clutter model for VHF SAR imagery

Julie Ann Jackson and Randolph L. Moses

The Ohio State University, Department of Electrical and Computer Engineering
2015 Neil Avenue, Columbus, OH 43210, USA

ABSTRACT

We present a physically-based clutter model for low frequency synthetic aperture radar that includes both distributed scatterers and large-amplitude discrete clutter. The model is used to generate a synthetic forest clutter scene comprised of two components, a background component and a heavy-tailed discrete component. Model parameters are based on characteristics of the scene, such as the radar cross-section of trees, forest thickness, and background radar cross-section. A synthetic SAR image of the scene is generated by modelling the radar imaging process as a lowpass filter and convolving the scene with the impulse response of the radar. We compare the synthetic, single-pass clutter image to measured data and present a metric for evaluating model fit. We also extended the model to describe correlated, multi-pass images for change detection applications.

Keywords: synthetic aperture radar, VHF, clutter, forest, change detection

1. INTRODUCTION

Interest in the detection of targets hidden by tree canopies has led to the development of foliage penetrating (FOPEN) radar. Although much of the FOPEN data collections are for UHF band synthetic aperture radar (SAR), some images have been collected using VHF SAR.[1,2] VHF band SAR is also of interest in forestry applications, such as the measurement of biomass.[3] For either application, characterization of VHF forest clutter is important for understanding the performance limitations of the radar.

Radar performance predictions, in terms of false alarm and detection probabilities, may be calculated from measured data. However, it is only possible to collect data for a limited number of scenes. It is of interest to understand radar clutter properties in order to simulate additional scenes, especially for operating conditions that differ from those for which measurements are available. Accurate detection performance predictions for these conditions require good scattering models for both targets and clutter.

Although clutter scattering has been well-studied for higher frequency radars,[4] less work has been reported for VHF. For UHF band, Mitra *et al.*, employ a joint scattering center and statistical model to describe clutter.[5] In this paper, we focus on forest clutter modelling at the VHF band and compare to measured data from the CARABAS SAR operated by the Swedish Defence Research Agency (FOI). We propose a physically-based method for producing synthetic forest clutter images. This model takes into account scene parameters and the correlation induced by the radar imaging process. We also extend the model to characterize radar clutter in change detection imagery.

We begin with a background discussion on popular density-fitting methods of clutter-modelling. Then, in Section 3, we present the physically-based model. The resulting clutter image is compared to measured data from the CARABAS SAR in Section 4. A quantitative metric of fit is also defined. In Section 5, we extend the model to the case of change detection images.

2. BACKGROUND

Studies of foliage backscatter have primarily used density-fitting methods to characterize the forest clutter.[1,6] It is common to match probability density functions to clutter backscatter magnitudes.[7]

Further author information: Send correspondence to Randolph L. Moses, E-mail: randy@ee.eng.ohio-state.edu

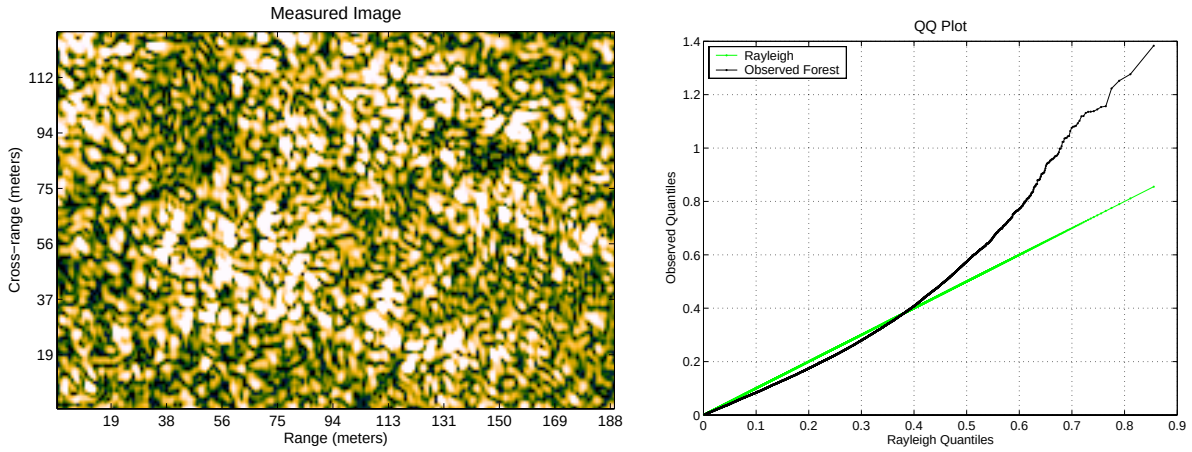

Figure 1. a) VHF SAR image of forest. b) Rayleigh QQ plot of forest data shown in a). Forest clutter has a heavier tail than Rayleigh-distributed clutter.

The Rayleigh density

$$f(x;\sigma^2) \quad = \quad \frac{x}{\sigma^2}\exp\left(-\frac{x^2}{2\sigma^2}\right) \tag{1}$$

has been widely used to characterize the magnitude of land clutter for homogeneous regions such as grass. The Rayleigh density models clutter for which a large number of independent scatterers are within the same resolution cell, provided that no one scatterer dominates the others.[8]

In forested regions, however, tree trunk scattering often dominates the scattering in a resolution cell. Therefore, the Rayleigh model no longer holds in these regions. Instead, a heavier-tailed distribution is needed to model the larger scatterers. Figure 1 shows a forested region in a VHF SAR image. The magnitude data is plotted versus Rayleigh quantiles on a quantile-quantile (QQ) plot. The QQ plot compares observed data to points with corresponding percentiles on a given distribution.[9] If the data comes from the given distribution, the resulting plot will be a line passing through the origin with slope one. Deviations from the unity-slope line indicate differences, such as heaviness of the probability density function (pdf) tail, between the expected distribution and that of the observed data. The upward curvature of the observed forest data in Figure 1b shows that the forest clutter magnitude data has a heavier-than-Rayleigh distribution tail.

Popular models for fitting to heavy-tailed distributions, such as those that arise in forest clutter, are the Weibull, log-normal, and K distributions. However, even these pdfs may fail to adequately describe forest clutter at low frequencies. Efforts have been made to use mixture density models[6] which describe the clutter as

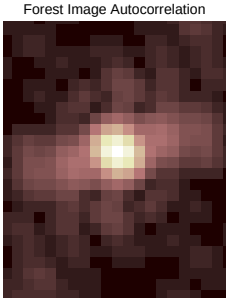

Figure 2. Autocorrelation of measured image shows pixel correlation.

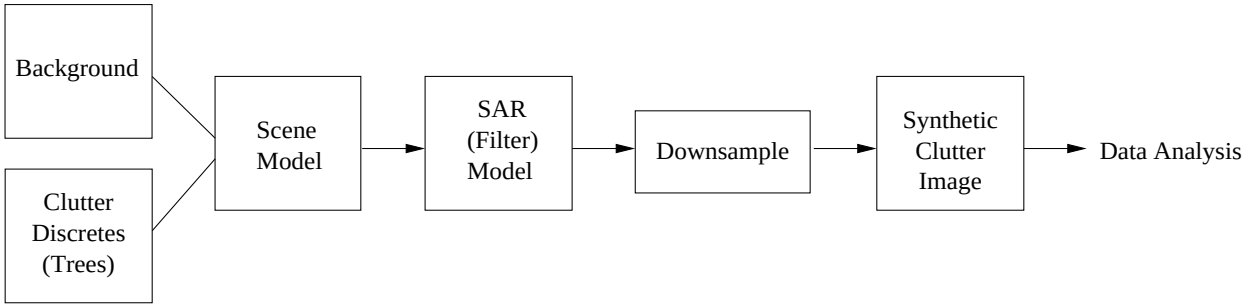

Figure 3. Clutter model derived from scene and radar characteristics.

combinations of small (Rayleigh) and large (heavy-tailed) scatterers. Such models may perform well in fitting a density function to the observed data. However, densities other than the Rayleigh generally lack a physical basis since the additional parameters are not derived from scene properties.[7] Another drawback of fitting density models is the assumption of independent image pixels that is often made, either explicitly or implicitly. Smith *et al.* note the effects of inter-tree interference on image texture for a model with just a few trees.[10] The autocorrelation of the measured image verifies that the pixels are not independent (see Fig. 2). In the next section, we propose a model that addresses both dependent pixels and a physical model basis.

3. CLUTTER MODEL

We propose a SAR clutter model that includes both a physical model for the clutter scene and a model of the SAR imaging process. The scene model contains two components. First, there is a background component that describes clutter backscatter that is distributed in the scene, and whose constituent scattering elements are spaced much more closely than the radar resolution. Examples of background scattering include grass, roads, *etc.* The second scene model component describes discrete, larger amplitude clutter such as tree trunks. The model is characterized by parameters that have a physical basis, such as the density of trees and a pdf of the tree trunk radar cross-section (RCS) amplitudes. The SAR imaging process is modelled as a linear filter applied to the image plane. Thus, we start with a scene model, then filter this scene by the SAR impulse response function in the image plane to obtain the final synthetic SAR image. The process is shown in Figure 3.

3.1. Scene model

Although the proposed model may describe any scene composed of background clutter along with large amplitude, discrete clutter, the scene of interest in this discussion is a forest. The forest scatterers are grouped into two categories—background and trees. The scene model takes into account the expected scattering statistics of trees and background as well as the forest thickness. An image model of the scene is formed from samples of the two types of scatterers.

The scene model is generated on the image (x, y) plane. The model applies to real-valued x (down-range) and y (cross-range) location parameters. However, since the model is typically simulated by computer, we discretize the (x, y) plane into a rectangular grid with index $[k, l]$ and spacing Δx and Δy in the x and y directions, respectively. The grid spacing is chosen to be small with respect to the SAR down-range and cross-range resolutions. We refer to points on the discrete synthesis grid as subpixels, since the filter output is downsampled to achieve a pixel image that represents the SAR image.

The scene background is assumed to be grass or other small scatterers such that the Rayleigh model in (1) holds for pixel magnitudes. Coherent processing of radar imagery requires the complex scattering information. Therefore, samples of the background clutter are generated as complex Gaussian noise. Each element of the discrete synthesis grid is thus a realization of an i.i.d. complex Gaussian random process. The resulting magnitude data will be Rayleigh-distributed with σ^2 as its parameter.[11] The variance σ^2 is related to background RCS as follows. The background RCS is typically reported as a magnitude value: σ_0 dB/m^2. We equate the image pixel

magnitude-squared values to RCS. So, in the synthesis grid, the complex pixel variance for a clutter cell with area $\Delta x \Delta y$ is $\sigma^2 = \sigma_0 \Delta x \Delta y$ dB. In general, we describe the background scattering as

$$B_{kl} = \alpha_{kl} + j\beta_{kl}, \tag{2}$$

where α and β are i.i.d. Gaussians with zero mean and variance σ^2). The parameter σ^2 is calculated from an estimate of the background RCS, σ_0, obtained from measured data and adjusted to compensate for the SAR filter model gain.

While the background contains small scatterers, the clutter discretes are assumed to be large scatterers such as trees that are randomly located in the scene. Because the tree scattering dominates in its subpixel cell, the Rayleigh model is not valid, and a heavy-tailed distribution is needed. There does not appear to be a validated physically-derived model for tree scattering available in the literature, although some modelling and validation of results has recently been reported.[12] In the absence of such a model, the log-normal pdf

$$f(x; \mu_t, \sigma_t^2) \quad = \quad \frac{1}{x\sqrt{2\pi\sigma_t^2}} \exp\left(-\frac{(\ln x - \mu_t)^2}{2\sigma_t^2}\right). \tag{3}$$

is chosen to model the magnitude of the tree scattering. The log-normal model has given reasonable clutter fitting results for data sets tested; the values of μ_t and σ_t have been estimated from these data sets. The parameters μ_t and σ_t describe variations due to environmental effects such as stem volume and ground slope. The complex scattering must also include a phase term. The phase is assumed to be uniformly distributed on $[0, 2\pi]$. This assumption is validated by analysis of measured data.

In addition to modelling the scattering statistics of the trees, the locations of the trees must also be determined. We assume Poisson placement with parameter λ, where λ is the tree density, or number of trees per square meter. The ground truth for the CARABAS data set includes tree density estimates; λ is set accordingly in the model.

Let $N = \lambda A_T$ be the total number of trees, where A_T is the total area of the clutter scene being modelled. Then, the tree scattering is characterized by

$$T_j = \{x_j, y_j, A_j, \phi_j\}, \quad j = 1, ..., N, \tag{4}$$

where x_j and y_j denote the coordinates of the tree, A_j is the log amplitude of the scattering, and ϕ_j is the phase. We discretize the tree scattering to the synthesis grid chosen above. Grid location $[k, l]$ is chosen to contain a tree with probability $p_t = \lambda \Delta x \Delta y$, and this choice is made independently for each grid location. If a given grid location is selected as containing the j^{th} tree, A_j is chosen from the pdf in (3) and ϕ_j is chosen from a uniform pdf over $[0, 2\pi]$. As discussed above, other models for the pdfs of A_j or ϕ_j could be used instead.

An example of the scene model is shown in Figure 4. The synthesis grid is first filled with samples from the background scattering distribution. Then trees are positioned by Poisson placement and scattering values assigned such that tree scattering replaces background scattering. Tree and background subpixels are taken to be independent of themselves and each other. The autocorrelation of the scene is then a single point in the two-dimensional space, *i.e.*, a delta function. Therefore, all correlation in the synthetic image is due to filtering with the SAR model.

3.2. System model

The synthetic aperture radar system is described by a two-dimensional linear filter, often called the impulse response (IPR) of the radar. The input to the filter is the scene scattering described above; the output image is the convolution of the input with the IPR. The filter is denoted $h(x, y)$. In order for the output image to be in units of RCS, the peak amplitude of $h(x, y)$ should be unity. In many cases a model of $h(x, y)$ is available from a system characterization of the radar.

For our model, we use a discretized sampling of $h(x, y)$, which we denote $h[k, l]$, where

$$h[k, l] = h(x, y) \text{ evaluated at } x = k\Delta x, \ y = l\Delta y \tag{5}$$

Thus, if $i[k, l]$ represents the input clutter image described in Section 3.1 and defined on the discretized grid $[k, l]$, the synthesized output SAR clutter image is given by

$$c[k, l] = i[k, l] * h[k, l]. \tag{6}$$

3.2.1. Estimating the IPR

If the impulse response of the SAR system is not given, it is possible to estimate it from background clutter regions in an output image. Assume we have available a measured region $c[m,n]$ from the radar system that contains background clutter only. We note that $[m,n]$ denotes the image pixel sampling, which may be different from the clutter discretization grid $[k,l]$ in equation (5). The filter's impulse response relates the autocorrelation of its input and output by

$$h[m,n] * h^*[-m,-n] * R_{ii}[m,n] \quad = \quad R_{cc}[m,n] \tag{7}$$

Taking the two-dimensional Fourier transform of (7) gives

$$|H(\omega_1,\omega_2)|^2 S_{ii}(\omega_1,\omega_2) = S_{cc}(\omega_1,\omega_2), \tag{8}$$

where S_{ii} and S_{cc} are the power spectral density functions of the input and output of the imaging process. Solving for H and taking the inverse transform yields the filter response. Since the phase information of the filter has already been lost, we can restrict the filter to be real-valued by taking the magnitude of the result. Thus, the radar system model is found to be

$$h[m,n] = \left| \mathcal{F}^{-1} \left(\sqrt{\frac{S_{cc}(\omega_1,\omega_2)}{S_{ii}(\omega_1,\omega_2)}} \right) \right|. \tag{9}$$

Given the power spectral densities of the system input and output, $h[m,n]$ may be computed directly from (9). The autocorrelation of the filter output may be calculated from the measured image $c[m,n]$. Then the power spectral density may be found via the Fourier transform. For the scene model established in Section 3.1, the input autocorrelation is a delta function. So, the power spectral density of the input is a constant value of one. Substituting into (9), the system response is found to be a unit gain lowpass filter. Since the filter is calculated on the pixel sampling grid $[m,n]$, it is necessary to convert the filter to the $[k,l]$ grid to match the input scene model sampling. Choosing the $[k,l]$ grid size to be a multiple of the pixel grid size allows for easy conversion via interpolation. Figure 5 shows the spatial response of the filter corresponding to the measured image in Figure 1.

4. CLUTTER SYNTHESIS RESULTS

In this section, we present results of synthesizing clutter to emulate clutter measured by the CARABAS SAR, which operates in the 20-90MHz band and uses HH polarization. A full description of the system may be found in Gustavsson *et al*.[13]

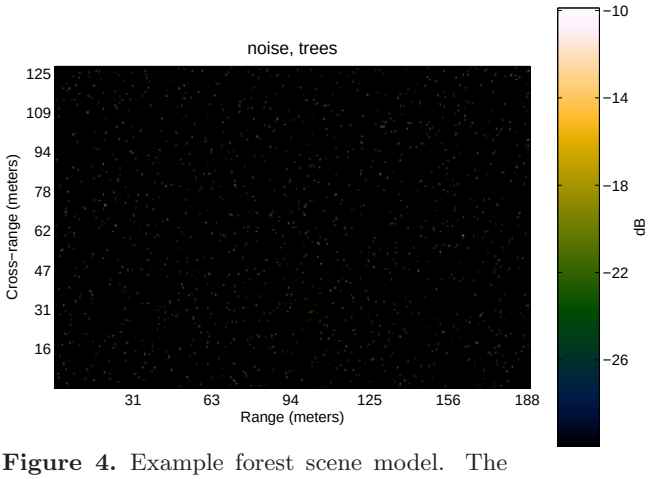

Figure 4. Example forest scene model. The white dots are the tree scattering points.

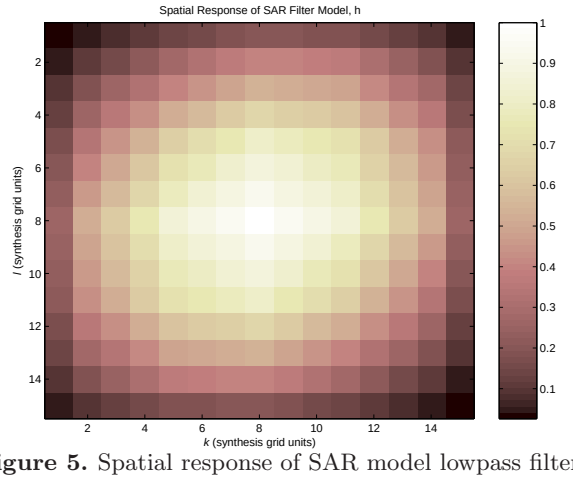

Figure 5. Spatial response of SAR model lowpass filter.

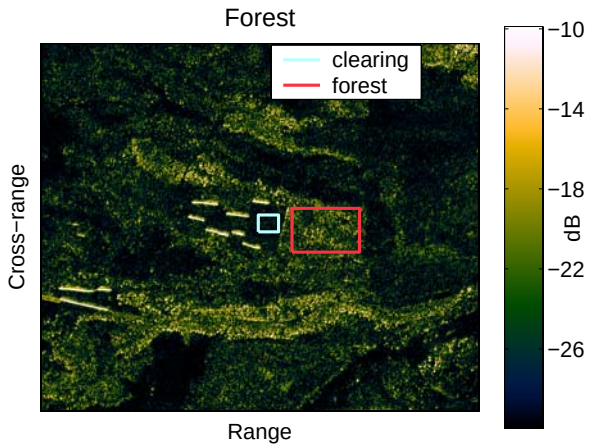

Figure 6. Regions of interest in CARABAS image.

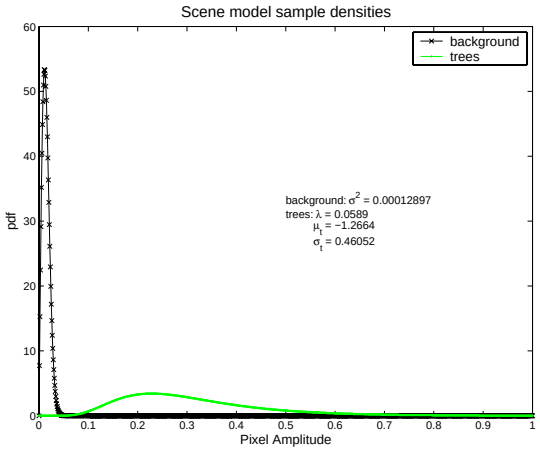

Figure 7. Scene model magnitude scattering pdfs.

4.1. Parameter selection

The image segment used in this study is one of a group of inventoried forest stands in Sweden. The radar resolution of the image is 3m×3m, while the pixel size is 0.9375m×0.9375m. The grid size for the scene model is chosen to be 3×3 subpixels per image pixel, which is approximately one-tenth the radar resolution in each dimension. The average diameter of tree in the forested scene is 0.26m. The ground-truth estimate of tree density is $\lambda = 0.0589$ trees/m^2.

The RCS of the background is estimated from a clearing near the forest in the measured image (Figure 6) to be $\sigma_0 = -21$dB. Dividing by the SAR filter gain, the corresponding Rayleigh parameter for the input background model is then found to be $\sigma^2 = 1.29 \times 10^{-4}$ (pixel amplitude units). Estimates for the tree scattering parameters are $\mu_t = -11\text{dB} = -1.2664$ (pixel amplitude units) and $\sigma_t = 4\text{dB} = 0.46052$ (pixel amplitude units). These estimates are not inconsistent with results of backscatter for large stem volumes (above 200m^3/ha) reported by Smith and Ulander.[12] The above parameter choices result in the model scattering densities shown in Figure 7.

4.2. Tests for clutter model fit

A visual comparison of measured and synthetic images is shown in Figure 8. The overall structure and magnitude response of the two scenes are comparable. Clearly, the measured image has more spatial variation than the synthetic image. A spatially varying tree density could easily be implemented in the model to obtain a more realistic synthetic image. However, for the application of detecting targets whose sizes are 1-2 times the image resolution, spatial variation in the clutter does not affect detection probabilities. So, more accurate modelling of the spatial variations is not needed for this application.

The exceedance function (one minus the cumulative distribution function) defines the probability of false alarm as a function of scattering magnitude thresholds. For accurate performance prediction estimates, the probability of false alarm for the synthetic clutter must match that of the measured image. Therefore, the exceedances must agree for magnitudes at a given threshold, τ.

The choice of threshold will depend on the expected target scattering and correspond to an accepted probability of a missed detection. Variations in acceptance levels and in target distributions will induce a prior distribution on τ, denoted $f_\tau(\tau)$. The distribution of τ will indicate an interval on the domain of the exceedance function where clutter model fit is of most importance. Therefore, we define a quantitative metric for testing clutter model fit to be the weighted squared-error between the synthetic and measured image exceedances, where the weighting is an expectation over τ. Denoting the error as ε, the error equation is

$$\varepsilon = \int |(1 - F_{meas}(\tau)) - (1 - F_{syn}(\tau))|^2 f_\tau(\tau)\, d\tau \quad (10)$$

$$= E\{|(1 - F_{meas}(\tau)) - (1 - F_{syn}(\tau))|^2\}, \quad (11)$$

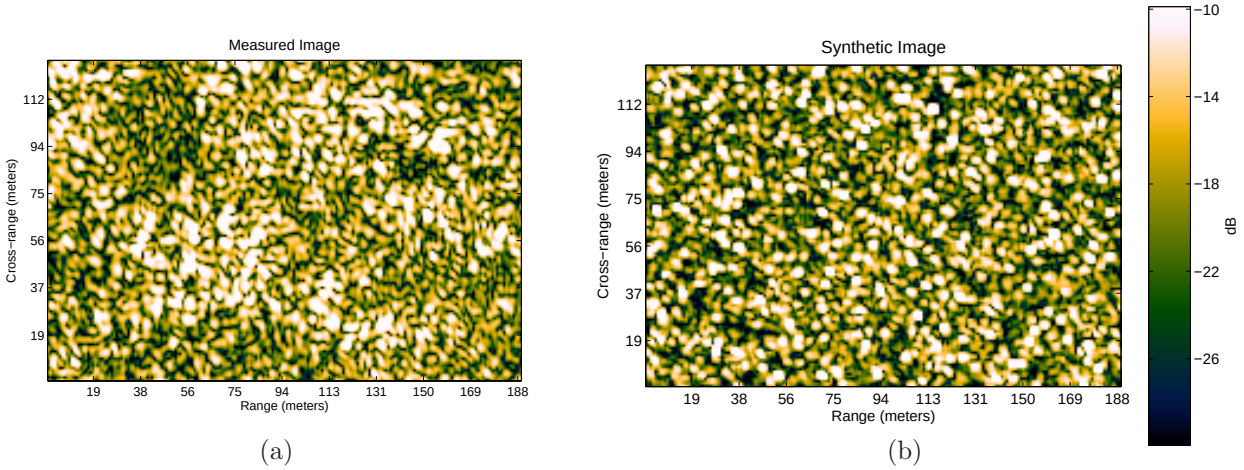

(a) (b)

Figure 8. Visual comparison of forest images: a) Measured image b) Synthetic image generated by clutter model.

where F_{meas} and F_{syn} are the cumulative distribution functions of the measured and synthetic magnitude data, respectively.

Figure 9 compares the exceedance plots for the synthetic model presented in this paper as well as the widely-used Rayleigh, Log-normal, and Weibull density-fitting models. Results from two choices of the synthetic model parameters are shown. The first synthetic model has parameters which closely match the ground truth. The second model assumes a much lower tree density and corresponding estimates of the tree scattering parameters. A prior density on τ is assumed to be Gaussian with mean 0.7 and variance 0.5^2, which we denote as $\mathcal{N}(0.7, 0.05^2)$. The errors computed with the metric in (11) are listed on the plots for each model, as well as in Table 1. The synthetic clutter model clearly outperforms the density-fitting models. At low magnitudes, the second model deviates from measured data; however, in the region of interest defined by the main lobe of $f_\tau(\tau)$ the two synthetic clutter models look very similar. In fact, the calculated error is only slightly less for the first model than the second for the given threshold distribution. Therefore, without having some *a priori* knowledge of the scene, such as the tree density, multiple solutions may exist. Performance of the solutions will differ depending on the choice of detection threshold.

Clutter Model	**Exceedance Error**
Synthetic Model 1	0.000046
Synthetic Model 2	0.000056
Best-fit Rayleigh	0.008613
Best-fit Log-normal	0.001386
Best-fit Weibull	0.003277

Table 1. Comparison of exceedance plot error values in Figure 9 for $f_\tau(\tau) \sim \mathcal{N}(0.7, 0.05^2)$.

5. EXTENSION TO CHANGE DETECTION

The synthetic clutter model proposed in Section 3 may be extended to model clutter in change detection images. Change detection images are formed by subtracting two images of the same scene, collected on multiple passes of the radar. Intuitively, stationary objects present in both images will cancel out in the subtraction. However, due to slight variations in the flight path, image alignment errors, environmental changes, *etc.*, stationary clutter will not be completely cancelled in the change detection image. Density-fitting models, which fit distributions directly to the change detection data, do not relate the collection variations in the single-pass images. Physically-based clutter models are advantageous because they are able to take into account the system and environmental changes.

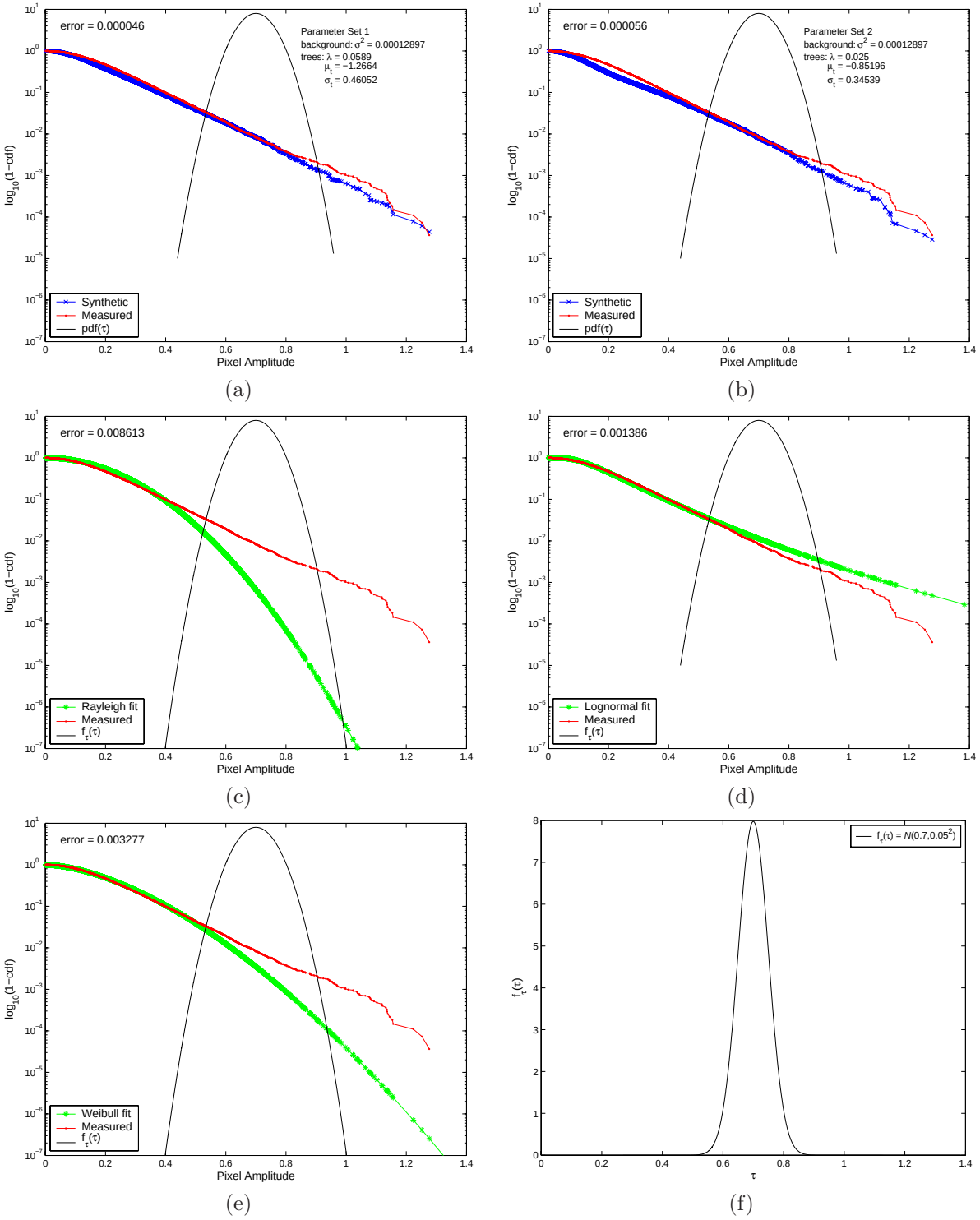

Figure 9. Comparison of measured data exceedance plots for several synthetic clutter models. (a) Proposed model with $\sigma^2 = 1.29 \times 10^{-4}$, $\lambda = 0.0589$, $\mu_t = -1.2664$, $\sigma_t = 0.46052$; these parameters closely match the ground truth. (b) Proposed model with $\sigma^2 = 1.29 \times 10^{-4}$, $\lambda = 0.025$, $\mu_t = -0.85196$, $\sigma_t = 0.34539$. (c) Best fitting Rayleigh model. (d) Best fitting Log-Normal model (e) Best fitting Weibull model. (f) Assumed prior pdf of detection threshold to obtain quantitative fit error numbers that are shown in the top left corner of (a)-(e).

5.1. Multi-pass clutter model

Although a complete characterization of the variations between radar passes is not known, we propose that a synthetic change detection image may be produced by subtracting two synthetic single-pass images, where the second image is a perturbation of the first. Section 3 described how to synthesize a single-pass clutter image. Here, we present a formulation of a second, correlated image.

A second-pass image is formed from small changes to the model parameters in the first-pass model. Letting a prime denote the second pass, the background representation becomes

$$B'_{kl} = \alpha'_{kl} + j\beta'_{kl} \tag{12}$$

where α'_{kl} and β'_{kl} may be correlated with α_{kl} and β_{kl} such that

$$\begin{pmatrix} \alpha_{kl} \\ \alpha'_{kl} \end{pmatrix}, \begin{pmatrix} \beta_{kl} \\ \beta'_{kl} \end{pmatrix} \sim \mathcal{N}\left(0, \begin{bmatrix} \sigma^2 & \rho\sigma^2 \\ \rho\sigma^2 & \sigma^2 \end{bmatrix}\right) \tag{13}$$

for correlation coefficient ρ. For $\rho = 0$ the background is uncorrelated from pass to pass and may be generated as independent complex Gaussian noise samples. However, the model above readily accommodates pass-to-pass correlated background clutter statistics, and so ρ is included here. Using the same prime notation, the trees in the second image are

$$T'_j = \{x'_j, y'_j, A'_j, \phi'_j\}, \quad j = 1, ..., N. \tag{14}$$

The changes in tree magnitude scattering are described as

$$A'_j = A_j + \gamma_j, \quad \gamma \sim f_\gamma(\gamma) \tag{15}$$

and the phase term is modified as

$$\phi'_j = \phi_j + \zeta_j, \quad \zeta_j \sim f_\zeta(\zeta). \tag{16}$$

In addition to variations in the scattering returns, the two single-pass images will also have some pixel misalignment. A tree pixel in one image may be displaced in the second image. The tree displacement is

$$\begin{pmatrix} x'_j \\ y'_j \end{pmatrix} = \begin{pmatrix} x_j \\ y_j \end{pmatrix} + \begin{pmatrix} \delta_{x_j} \\ \delta_{y_j} \end{pmatrix}, \quad \begin{pmatrix} \delta_{x_j} \\ \delta_{y_j} \end{pmatrix} \sim f_\delta(\delta). \tag{17}$$

Forming a second-pass image from the perturbation equations above simulates the system and environmental changes between two measured images. Once the two single-pass images have been formed, one can obtain the synthetic change detection image by either coherent or incoherent subtraction.

Although the above model has been generated for two related images, the model is easily generalized to the case of three or more correlated images. Thus, the change detection model extends to multi-pass applications.

5.2. Change Image Simulation Example

We illustrate the above multi-pass model with example synthetic imagery. We take the first pass model to be the single-pass example in section 4. A second, correlated model is generated as follows. We assume that the difference in tree location between images is normally-distributed with zero mean and a standard deviation of 0.5m. The location change would primarily be due to registration errors of the two images. We assume the tree magnitude varies by a zero-mean normal distribution with a standard deviation of 2.5% of the median magnitude in the first image. Also, assume that phase changes are negligible so that equation (16) becomes $\phi'_j = \phi_j$. Finally, let the background scattering between images be uncorrelated by setting $\rho = 0$ in equation (13).

After filtering the correlated, single-pass models with the SAR system model and downsampling, we obtain the pair of synthetic clutter images shown in Figures 10a and 10b. The two single-pass images are subtracted both coherently (Figure 10c) and incoherently (Figure 10d) to obtain change detection images. It is common in change detection images to plot either the arrivals or departures from a scene. Arrivals are defined to be those

pixels corresponding to positive incoherent subtraction results, while departures are those pixels corresponding to negative incoherent subtraction results. The synthetic change detection images in Figure 10 show arrivals to the scene; departure images are similar. Ideally, large discrete clutter will completely cancel, leaving only small residuals in the change detection images. However, Figure 10 clearly shows that amplitude and spatial variations between the two single-pass images leave some large residual scattering in the change detection images. A comparison of the exceedance plots for both the single-pass and change detection images (Figure 11) shows that the peak magnitude of the residual scattering is approximately half the peak magnitude of the single-pass scattering. We observe that the incoherent change detection image in this example has greater cancellation than the coherent change detection image. Unfortunately, no publicly releasable change detection images were available for comparison with the results in Figures 10 and 11.

6. CONCLUSION

In this paper, we have presented a physically-based clutter model that includes both distributed (background) scatterers and large-amplitude discrete clutter, such as trees. A synthetic forest model is proposed. The model parameters are obtained from a physical understanding of the scene. Tree size and forest thickness relate to the tree RCS amplitudes. Background RCS is also taken into account. Synthetic SAR images of the model scene

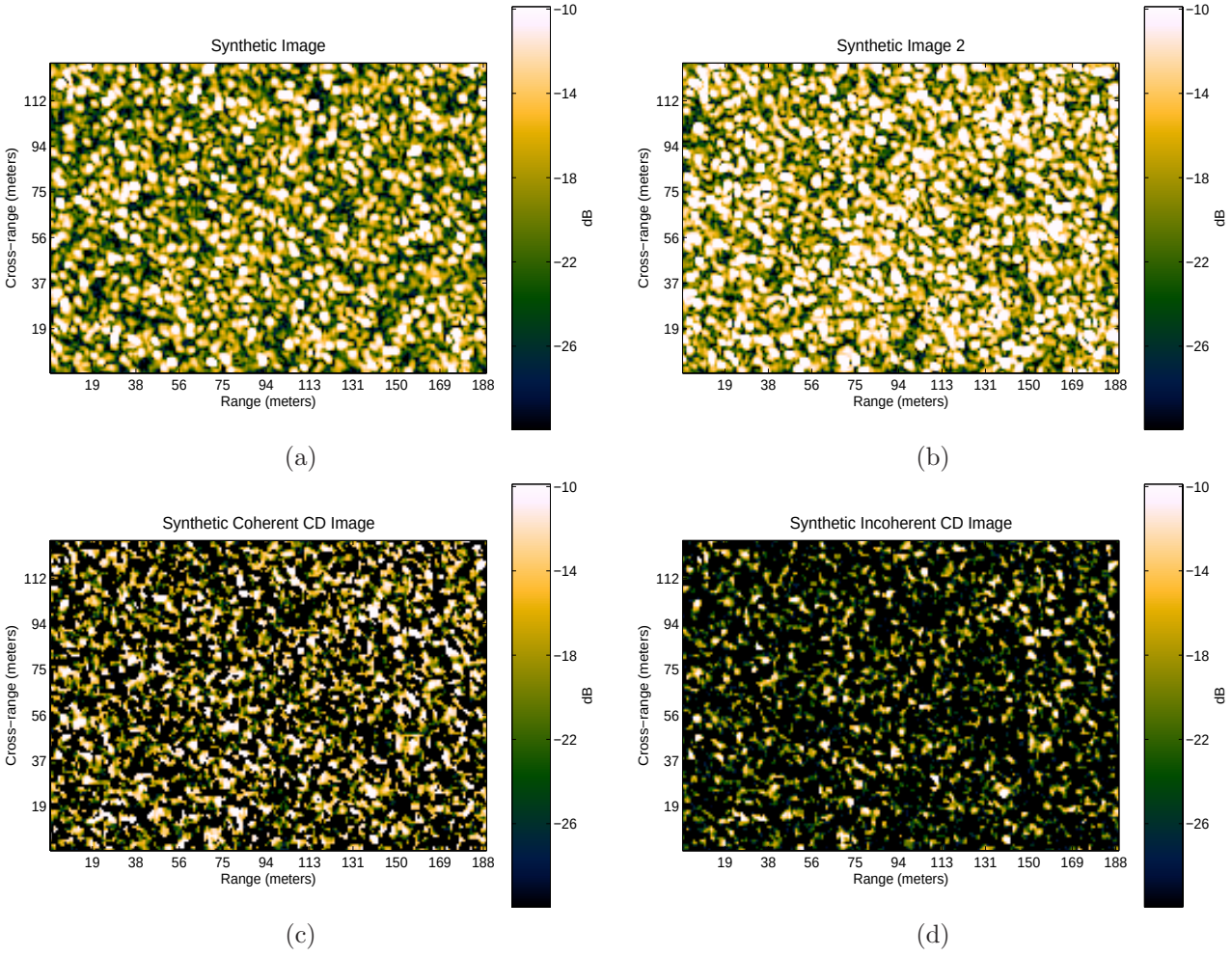

Figure 10. (a) Synthetic single-pass image. (b) Perturbation of the image in (a). (c) Coherent change detection image formed from the images in (a) and (b). (d) Incoherent change detection image formed from (a) and (b).

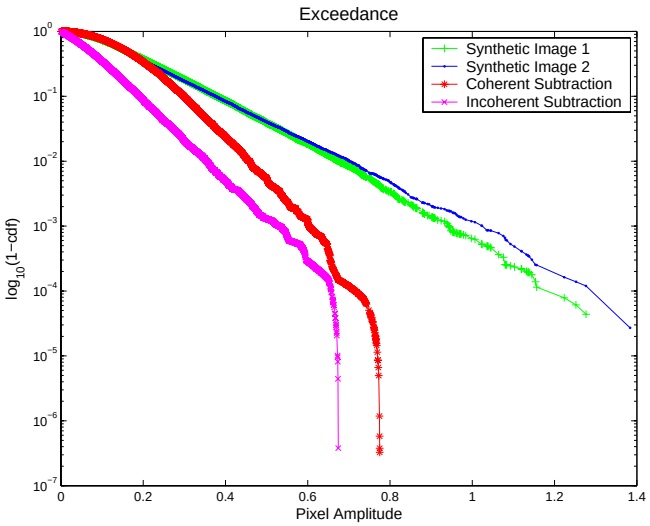

Figure 11. Exceedance plots for synthetic multi-pass and change detection images.

are generated by convolving the scene with the impulse response of the radar. An estimation method was given for the case when the radar impulse response is unknown. We have shown that the single-pass synthetic clutter images agree well with CARABAS SAR measurements. We have also extended the model to the case of change detection images. Two-pass (or multi-pass) images may be modelled as correlated scenes, where the second image is a perturbation of the first. Perturbation parameters model how large the changes are in environment and data collection geometry between passes. Inclusion of these variations in the clutter model provides a physically-based description of both single-pass and multi-pass images.

ACKNOWLEDGMENTS

The authors would like to thank the Swedish Defence Research Agency (FOI) for providing the CARABAS SAR data. The material in this paper is based upon work supported under a National Science Foundation Graduate Research Fellowship and funding from the Dayton Area Graduate Studies Institute (DAGSI).

REFERENCES

1. L. Bessette and S. Ayasli, "Ultra-wideband P-3 and CARABAS II foliage attenuation and backscatter analysis," *Proc. IEEE Int. Radar Conf.*, pp. 357–362, 2001.
2. B. Binder, M. Toups, S. Ayasli, and E. Adams, "SAR foliage penetration phenomenology of tropical rain forest and northern U.S. forest," *Proc. IEEE Int. Radar Conf.*, pp. 158–163, 1995.
3. J. E. Fransson, F. Walter, and L. Ulander, "Estimation of forest parameters using CARABAS-II VHF SAR data," in *Transactions on Geoscience and Remote Sensing*, **38**(2), pp. 720–727, March 2000.
4. M. Long, *Radar Reflectivity of Land and Sea, 3rd Ed.*, Artech House, Boston, 2001.
5. A. Mitra, T. Lewis, A. Paul, and A. Shaw, "Self-training algorithms for ultra-wideband radar target detection," in *Algorithms for Synthetic Aperture Radar Imagery X*, E. G. Zelnio and F. D. Garber, eds., *Proceedings of SPIE* **5095**, pp. 254–264, 2003.
6. E. Blasch and M. Hensel, "Fusion of distributions for radar clutter modeling," *Proc. of Int. Conf. on Information Fusion*, June 28-July 1, 2004, Stockholm, Sweden.
7. C. Oliver and S. Quegan, *Understanding Synthetic Aperture Radar Images*, Artech House, Boston, 1998.
8. M. Skolnik, *Introduction to Radar Systems, 3rd Ed.*, McGraw Hill, New York, 2001.
9. H. C. Thode Jr., *Testing for Normality*, Marcel Dekker, Inc., NY, 2002.

10. G. Smith, L. Ulander, and J. Askne, "VHF backscatter sensitivity to forest properties: Model predictions," in *Proc. IGARSS'99*, pp. 1889–1891, 1999.
11. H. Stark and J. W. Woods, *Probability and Random Processes with Applications to Signal Processing, 3rd Ed.*, Prentice Hall, Upper Saddle River, NJ, 2002.
12. G. Smith and L. Ulander, "A model relating VHF-band backscatter to stem volume of coniferous boreal forest," in *IEEE Trans. on Geoscience and Remote Sensing*, **38**(2), pp. 728–740, March 2000.
13. A. Gustavsson and P. Frölind *et al.*, "The airborne VHF SAR system CARABAS," in *Proc. IGARSS'93*, pp. 558–562, 1993.